Microchemical Journal 200 (2024) 110314

Contents lists available at ScienceDirect

Microchemical Journal

journal homepage: www.elsevier.com/locate/microc

Non-enzymatic glucose sensor using mesoporous carbon screen-printed electrodes modified with cobalt phthalocyanine by phase inversion

María-Isabel González-Sánchez [a], Hanen Khadhraoui [a,b], Rebeca Jiménez-Pérez [a], Jesús Iniesta [c], Edelmira Valero [a,*]

[a] Universidad de Castilla-La Mancha (UCLM), Department of Physical Chemistry, Higher Technical School of Industrial Engineering, 02071 Albacete, Spain
[b] Université de Carthage, Faculté des Sciences de Bizerte, LR01 ES15, Laboratoire de Physique des Matériaux: Structure et Propriétés, 7021 Zarzouna, Bizerte, Tunisia
[c] Universidad de Alicante, Department of Physical Chemistry and Institute of Electrochemistry, 03690-San Vicente del Raspeig, Alicante, Spain

ARTICLE INFO

Keywords:
Mesoporous carbon
Cobalt phthalocyanine
Phase inversion
Screen-printed electrodes
Glucose sensor
Non-enzymatic sensing

ABSTRACT

The development of non-enzymatic glucose electrochemical sensors is still required to be used for the determination of glucose in complex biological media. This study presents a straightforward and remarkably efficient tool for the preparation of highly stable and sensitive glucose electrochemical sensors based on the deposition of cobalt phthalocyanine (CoPc) onto mesoporous carbon screen-printed electrodes (MCs). Results show that the MC electrochemical activation (aMC) followed by phase inversion (PI), which consisted of drop casting of CoPc in dimethylformamide onto a wetting electrolyte leading to the electrode aMC-CoPc/PI, enhanced sensitivity towards glucose determination in complex media. The beneficial need for MC surface activation and PI has been explored by scanning electron microscopy, energy dispersive X-ray spectroscopy, Raman spectroscopy, cyclic voltammetry and electrochemical impedance spectroscopy. The aMC-CoPc/PI electrode exhibited the highest electrocatalytic activity of the series (namely, MC-CoPc, MC-CoPc/PI and aMC-CoPc) towards glucose oxidation. By using square wave voltammetry technique, the aMC-CoPc/PI glucose electrochemical sensor demonstrated a sensitivity of 22.3 μA mM^{-1} and a low detection limit of 27.4 μM (S/N = 3) in a linear dynamic range of 0.1 to 3.5 mM. Additionally, it also displayed high selectivity, robust stability, repeatability and reproducibility toward the quantification of glucose concentration in complex samples such as horse serum, intravenous glucose saline solution and culture medium for sperm cells.

1. Introduction

Metallophthalocyanines (MPcs) are an attractive class of macrocyclic complex compounds widely known for their outstanding electrocatalytic activities towards the oxidation of a plethora of chemical substances [1–3]. Among the MPcs, cobalt phthalocyanine (CoPc) has been extensively used as a mediator in electronic devices because of its rich redox chemistry and adequate electron transport capability, which has led to its wider applications in low-overpotential sensors fabrication [4,5]. Nevertheless, a drawback associated with the physical adsorption of MPcs on electrode surfaces is the lack of physical stability of MPc adsorbed species as they usually peel off from the electrode surface, resulting in a decrease of electrochemical activity [6]. Hence, an adequate selection of the support material is essential to gain stability and good performance of MPc-based electrochemical sensors. Since MPcs exhibit a highly conjugated π-electron system that can interact with carbon nanomaterials through π-π stacking [7], the use of carbon materials is suitable to enhance the adsorption-immobilization of MPcs.

Mesoporous carbon (MC), with a distribution of pores in the range of 2 to 50 nm [8], displays important properties such as controlled pores size and distribution, high electroactive area, high capacity to host a wide variety of electrocatalysts and good chemical stability [9,10]. As a result of these distinctive properties, MCs have found widespread applications in electrochemistry, including energy storage in supercapacitors and batteries, catalysis in reactions like oxygen reduction and hydrogen evolution, adsorption of pollutants from water and air [11], as well electroanalytical applications where MCs act as support [12]. As far for electrochemical sensing, MC has even shown more favorable electron transfer kinetics than carbon nanotubes (CNTs) [13]. The high density of edge plane-like defective sites and the relatively large surface area may

* Corresponding author.
E-mail addresses: Misabel.Gonzalez@uclm.es (M.-I. González-Sánchez), Rebeca.Jimenez@uclm.es (R. Jiménez-Pérez), Jesus.Iniesta@ua.es (J. Iniesta), Edelmira.Valero@uclm.es (E. Valero).

https://doi.org/10.1016/j.microc.2024.110314
Received 6 December 2023; Received in revised form 15 February 2024; Accepted 10 March 2024
Available online 11 March 2024

provide many favorable sites for electron transfer as well for immobilization of electrocatalytic substances [14,15]. Furthermore, it has been shown that the inherent nanoarchitecture of MC surface improves dispersion and distribution of nanoparticles, thereby enhancing substrate binding, mobility, and collision probability [16,17].

Phase inversion (PI) is a technique that has been successfully applied for the immobilization of enzymes, metal nanoparticles, CNTs and zinc phthalocyanines into polymeric membranes [18–21]. In a typical PI procedure, a polymer is dissolved in a water-miscible organic solvent (casting solution). After distributing that suspension onto the surface of interest, an aqueous solution is added on the polymer suspension. As the polymer is insoluble in water, the addition of this solution induces its precipitation [20]. PI has been also employed for the preparation of carbon-based materials with different applications; as a case in point, a modified PI process was employed to prepare 3D graphene embedded with nitrogen-doped carbon nanoparticles for application in supercapacitors [22]. In another interesting study, PI was used to prepare porous carbon for lithium-sulfur battery cathodes [23]. PI has been also used to modify commercial screen-printed electrodes (SPEs) using polysulfone membranes [19,21,24–26].

Therefore, this work aims to assess the effectiveness of a modified PI procedure in the presence of salt as a cost-effective methodology for the immobilization/adsorption of CoPc into activated MC-based screen-printed electrodes. The modified procedure was expected to improve the electroanalytical outcome and stability of the electrodes, making them suitable for glucose electrochemical sensing in complex media. The continuous and rapid monitoring of glucose concentration in body fluids, cell culture media or foodstuffs is crucial to avoid any possible complication affecting human health or cell development. For that, there has been substantial interest in developing and improving glucose electrochemical (bio)sensors [27–30]. Over the last decade, some CoPc-based enzyme-free glucose sensors have been developed using nanohybrid materials such as multiwalled carbon nanotubes/cobalt tetrasulfonated phthalocyanine [31], CoPc/ionic liquid/graphene [32] or CoPc/single-walled carbon nanotube/reduced graphene oxide [33] with good performance. However, these works required the presence of advanced and expensive conductive carbon nanostructures and/or ionic liquids to improve the electrochemical response.

In the present work, a novel, simple and highly efficient method for the preparation of a glucose electrochemical sensor to be used in complex media has been designed. The change in surface chemistry of MC by a straightforward electrochemical activation has been proven as a key parameter for the optimum adsorption of CoPc on the MC network. Under MC surface modification and PI application for CoPc adsorption, the outcome of the glucose electrochemical sensor was determined by square wave voltammetry. The CoPc-based glucose electrochemical sensor exhibited good electroanalytical parameters towards glucose measurement in prepared solutions and some complex real samples, such as horse serum, intravenous glucose saline solution and culture medium for sperm cells.

2. Materials and methods

2.1. Reagents

L-ascorbate sodium salt, citric acid trisodium salt, cobalt (II) phthalocyanine (CoPc), L-dehydroascorbic acid (DHA) sodium salt, N,N-dimethylformamide (DMF), dopamine, D-(+)-glucose, sucrose, urea and uric acid sodium salt were purchased from Sigma Aldrich (Madrid, Spain). Potassium hexacyanoferrate(II) trihydrate, sodium chloride and sodium hydroxide were from Merck (Madrid, Spain). Solutions were freshly prepared every day with deionized water (resistivity no less than 18.2 MΩ·cm at 25 °C) (Millipore, Watford, UK). A commercial glucose assay kit based on the enzymatic oxidation of glucose by the enzyme glucose oxidase was purchased from Sigma-Aldrich. This is a bi-enzymatic assay in which glucose is oxidized to gluconic acid by glucose oxidase, also yielding hydrogen peroxide, which then reacts with *o*-dianisidine in the presence of peroxidase to yield a colored product at an acidic pH to be measured at 540 nm. Spectrophotometric measurements were performed according to the supplier's instructions (https://www.sigmaaldrich.com/ES/es/product/sigma/gago20).

2.2. Preparation of modified electrodes

Screen-printed carbon electrodes (SPCEs) modified with mesoporous carbon from Metrohm-Dropsens (DRP-110MC, MCs) were used for the present study. The electrodes consisted of a mesoporous carbon/carbon ink working electrode with a geometrical area of 12.6 mm^2, a carbon ink counter electrode and a silver ink pseudo-reference electrode.

The preparation of modified electrodes is illustrated in Scheme 1. Firstly, MCs were pre-treated by cyclic voltammetry from 1.0 to −1.0 V at 0.05 Vs^{-1} in 0.1 M NaOH for one cycle to generate the activated electrodes (aMCs). Then, two different ways of immobilizing CoPc based on drop casting were carried out: 1) without PI and 2) with PI. In the first case, 2 μL of a solution of CoPc (2.5 mg/mL in DMF) was directly drop casted onto the working electrode of MCs and aMCs to obtain MC-CoPc and aMC-CoPc electrodes, respectively. In the second strategy, the electrodes were immersed in a solution containing 0.1 M KCl for 1 h; then, the electrodes were placed on a flat surface to modify the working electrode with CoPc. For that, 5 μL of an aqueous solution 0.1 M KCl were drop casted onto the MC and aMC working electrodes. Subsequently, 2 μL of a solution of CoPc (0–5 mg/mL in DMF) was drop casted onto the solution of KCl to induce precipitation and immobilization of CoPc and favor its adsorption on the mesoporous network (phase inversion). The electrodes obtained by this method were named as MC-CoPc/PI and aMC-CoPc/PI, respectively. After drop casting of CoPc, the electrodes were allowed to dry in the air at room temperature (RT).

2.3. Electrochemical measurements

The electrochemical experiments were carried out with an AUTOLAB potentiostat PGSTAT 128N controlled by the NOVA 2.0 software package equipped with an EIS analyzer (Eco Chemie B.V., Utrecht, The Netherlands). Unless otherwise indicated, all indicated potentials are referred to the Ag pseudo-reference electrode of the screen-printed platforms. The experimental conditions used are specified in the corresponding figure captions. All electrochemical measurements were performed in a 10-mL cell at RT (25 ± 2 °C), with no deaerated solutions. EIS experimental conditions were the following: the electrodes were polarized at 0.2 V for 30 s. Then, a sinusoidal amplitude potential perturbation (5 mV rms) was imposed between 65 kHz and 10 mHz, with ten points per decade. Square wave voltammetry (SWV) measurements were preceded by the application of a doble potential step chronoamperometry at –0.7 V during 5 s and 0 V during 5 s. SWV measurements were performed with a modulation amplitude of 50 mV, a frequency of 2.5 Hz and a step of 5 mV.

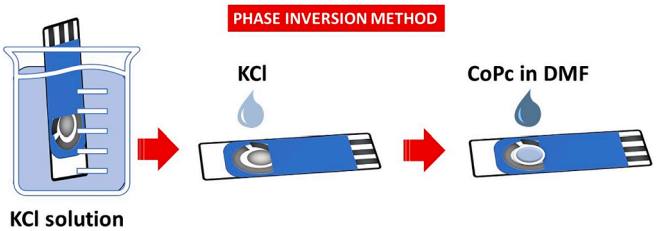

Scheme 1. Depiction of the preparation of the electrodes by phase inversion (PI).

2.4. Physicochemical measurements

The morphology of the electrodes was analyzed using field emission scanning electron microscopy (FE-SEM, HITACHI S-3000 N microscope), working at 30 kV with a Bruker X flash 3001 X-ray detector for the microanalysis.

The XPS experiments were recorded on a K-Alpha Thermo Scientific spectrometer using Al-Kα (1486.6 eV) radiation, monochromatized by a twin crystal monochromator, yielding a focused X-ray spot with a diameter of 400 μm mean radius. The alpha hemispherical analyzer was used as an electron energy analyzer, operating in fixed analyzer transmission mode, with a survey scan pass energy of 200 eV and 40 eV narrow scans. The angle between the X-ray source and the analyzer (magic angle) was 54.7°. Avantage software was used for processing the XPS spectra, with energy values referenced to the C1s peak of the adventitious carbon located at 284.6 eV, and a Shirley-type background.

Spectrophotometric measurements were carried out using a UV/Vis Perkin-Elmer Lambda 35 (Perkin Elmer Instruments, Waltham, USA) spectrophotometer at 25 °C. Raman spectroscopy measurements were carried out using a JASCO NRS-5100 Laser Raman spectrometer coupled with a confocal microscope (×50 objective). The excitation line was provided by a standard laser at 532 nm at a very low power level to avoid heating effects.

2.5. Real samples

The real samples herein tested consisted of horse serum, intravenous glucose saline solution and culture medium for sperm cells. Horse serum was from Sigma-Aldrich (reference H1270) and the intravenous glucose saline solution was purchased from a local pharmacy (with a composition of 0.9 % w/v NaCl and 5 % w/v glucose). The culture medium for sperm cells was generously supplied by the Health and Biotechnology research group (University of Castilla-La Mancha, Spain) with the following chemical composition: Tris (27 g·L^{-1}), citric acid (14 g·L^{-1}), glucose (10 g·L^{-1}) and clarified egg yolk (20 % v/v) [34]. All samples were diluted in aqueous NaOH 0.1 M for the electrochemical measurements. Both the culture media for sperm cells and horse serum were deproteinized before the measurements. To do that, samples with the appropriate dilutions were introduced into a water bath at 90 °C for 10 min. Afterwards, solutions were centrifuged at 6,000 rpm for 10 min and the supernatant was filtered and collected.

For the electrochemical measurement of real samples, a drop of the sample (about 20 μL) was placed on the surface of the electrodes. The measurements were carried out by SWV with the parameters previously indicated (see 2.3. Electrochemical Measurements). All the measurements were compared with a standard enzymatic spectrophotometric method (see Reagents) and assays were performed in triplicate.

3. Results and discussion

3.1. Characterization of the electrodes

Commercial SPCEs are fabricated using inks that sometimes require activation to improve electron transfer and enhance sensing performance [35,36]. This is due to the existence of some organic solvents, binding pastes and some additives that can lead to sluggish kinetics. Electrochemical pretreatments of SPEs allow the *in-situ* activation of working electrodes [37,38]. In this work, MCs were pretreated by cyclic voltammetry in 0.1 M NaOH. To determine if some functionalities were introduced on the surface of the electrodes during the activation process, XPS analysis was conducted (Figs. 1 and S1). Analysis of C1s and O1s core level spectra analysis revealed important modifications of carbonaceous inks of MCs after activation. XPS deconvolution of the C1s core level spectrum (Fig. 1A and B) showed the presence of peaks at 284.6, 285.6, 286.5 and 288.7 eV, which were assigned to graphitic C-C, aliphatic C-C and/or C-H and/or C-N, C-O and C=O, respectively [39]. XPS deconvolution of O1s core level spectrum (Fig. 1D and E) exhibited energy peaks at 532.2, 533.2 and 534.3 eV, attributed to C=O, C-O and C-OH groups, respectively [39]. The high resolution for the analysis of C1s and O1s spectra revealed a decrease in carbon content (95.5 % for

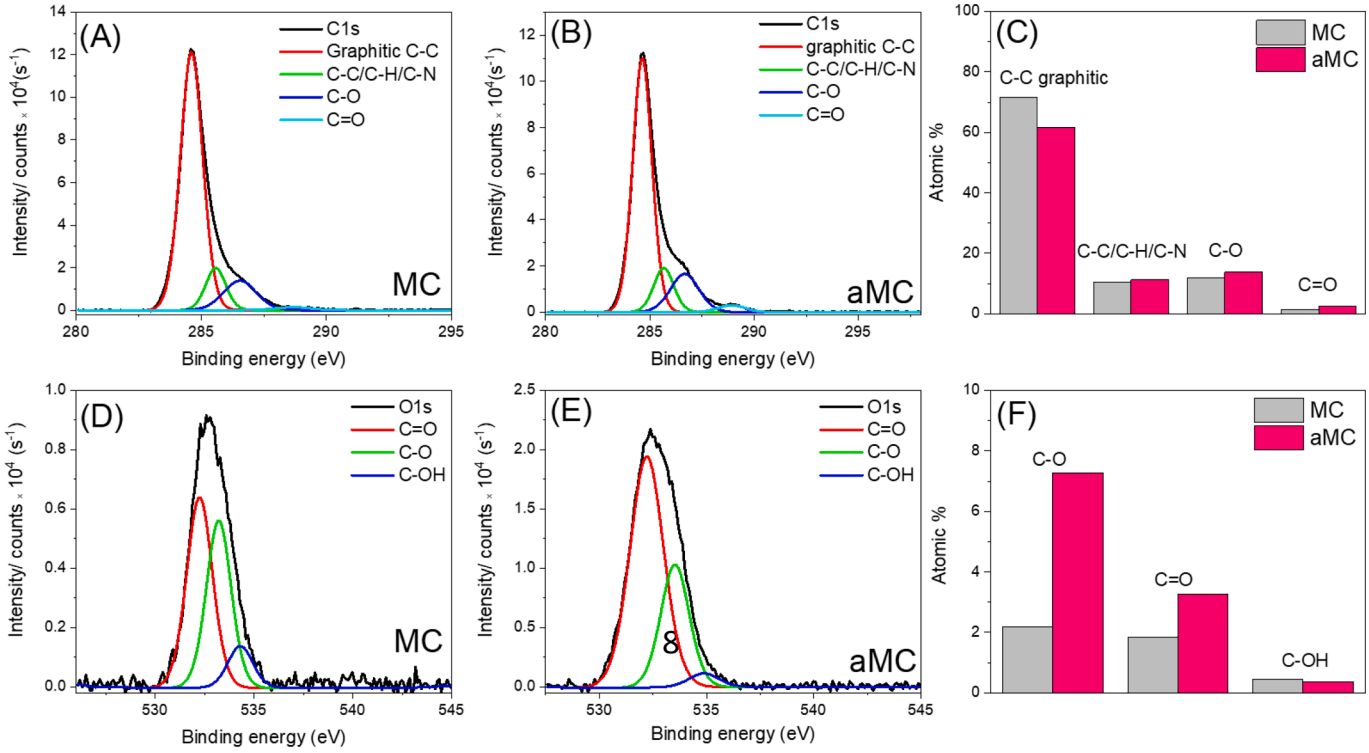

Fig. 1. XPS spectra C1s for MC (A) and aMC (B). (C) Atomic % of functional groups after deconvolution of C1s atomic level. XPS spectra O1s for MC (D) and aMC (E). (F) Atomic % of functional groups after deconvolution of O1s.

MC, 89 % for aMC) as well an increase in oxygen content (4.5 % for MC, 11 % for aMC). After activation, graphitic C-C atomic % decreased whereas the oxygenated species (C-O and C=O) atomic % increased, as shown in detail in Fig. 1C and F. As a result, the functionalization of MCs with polar oxygen-containing functional groups provides a more hydrophilic character to the electrode surface and, therefore, better wettability.

Fig. 2 displays the SEM of surface morphology of MC, aMC, MC-CoPc, aMC-CoPc, MC-CoPc/PI and aMC-CoPc/PI. Firstly, when MC and aMC are compared (Fig. 2A and B), the photographs show a more open porosity in the case of aMC, which would indicate a cleaning of carbon surface by NaOH, probably due to the removal of organic binders or other non-electroactive materials [37,38]. After drop casting with CoPc (Fig. 2C-F), SEM results revealed heterogeneous surfaces containing microcrystals of CoPc with tubular morphology stacked on the electrode surface. Larger and more ordered microcrystals can be appreciated in the case of electrodes modified by PI (Fig. 2E and F) compared with those electrodes modified without PI (Fig. 2C and D), which exhibit a more unequally and messy CoPc film deposition. Interestingly, SEM-EDX color mapping of the electrodes (Fig. S2) revealed higher content and better distribution of CoPc in the previously activated electrode modified with PI (aMC-CoPc/PI, Fig. S2D).

Therefore, to corroborate these results, CVs at different scan rates were performed in NaOH for an estimation of the electroactive species concentration on the surface of the electrodes (Γ) (Fig. S3), using the following equation [41]:

$$Ip = \frac{n^2 F^2 \nu A \Gamma}{4RT} \quad (1)$$

where n is the number of electrons transferred (1 electron), F the Faraday constant (96485.33 $C \cdot mol^{-1}$), ν the scan rate, A the geometrical area, R the ideal gas constant (8.31 $J \cdot mol^{-1} \cdot K^{-1}$) and T the temperature. The Γ values obtained were $1.26x10^{-10}$, $2.25x10^{-10}$, $2.02x10^{-10}$ and $2.58x10^{-10}$ $mol \cdot cm^{-2}$ for MC-CoPc, MC-CoPc/PI, aMC-CoPc and aMPC-CoPc/PI, respectively, which clearly indicate that electrodes previously activated and modified with PI had a higher amount of immobilized CoPc than the other electrodes. These results could be due to the increase in surface energy of the electrode as a consequence of the activation (by introduction of polar oxygen functional groups on the mesoporous carbon) and to the presence of the salt, which has been shown to be accompanied by a stronger adsorptive behavior [40]. Additionally, this fact could result in CoPc molecules lying flat on the surface and that their central cobalt atom forming a chemical bond with oxygen ions [41], leading to more efficient adsorption of the CoPc molecule. The corresponding plots of the anodic peak currents linearly increased with the scan rate (insets in Fig. S3), which confirms surface-controlled electrochemical processes.

Raman spectroscopy was used to evaluate changes on the surface of the electrodes before and after modification (Fig. 3). Spectra for MC and aMC surfaces (Fig. 3A and B) showed typical features of carbonaceous materials in the Raman shift between 1200 and 1800 cm^{-1}. In the case of MC, the disorder-induced tangential stretching vibrational band (D) and the in-plane (sp^2 hybridized) vibrational mode (G) were observed at 1332 and 1574 cm^{-1}, respectively. These results revealed some disordered forms of graphitic carbon structure present in the walls of MC [42]. A broad second order 2D band at 2674 cm^{-1} presents the first overtones of D band, which is attributed to multiple layers of graphene in graphite structure [43]. After activation of the MC electrode, Raman spectra revealed a small shift of 5 cm^{-1} in D and G bands (1337 and 1579 cm^{-1}, respectively) and an increase of 40 cm^{-1} in the 2D band (2714 cm^{-1}). Shifts in both D and G bands can be indicative of structural stress on carbon bonding due to the introduced heterogeneous atoms and charge carriers on the surface [44]. It has been reported that the addition of oxygen to graphitic carbon leads to an increase in the Raman shift of the D-band [45]. Moreover, an upshift in the G-band is related to the incorporation of a charged dopant, which modifies charge carriers' concentration at the surface [46]. A red shift of the 2D-band indicates the introduction of charge induced by electrons [47]. All these results point to the introduction of oxygenated functional groups on the surface of the electrodes, as confirmed the XPS results previously obtained (Fig. 1).

Furthermore, the intensity ratio of D to G bands (I_D/I_G) is commonly used to measure the quality of graphitization in crystalline graphite [48]. The I_D/I_G values obtained were 0.86 and 0.78 for MC and aMC, respectively. In both cases, the high I_D/I_G values obtained indicate the presence of defects, such as vacancies or grain boundaries, typical of a roughed material. The lower I_D/I_G found in aMC could indicate an increase in the average sizes of the sp^2 domains and a slight reduction of defects degree when electrodes are activated [49]. This fact could be consistent with a cleaning of the surface by removal of organic binders and other impurities.

Raman spectra of aMC, CoPc and aMC-CoPc/PI are shown in Fig. 3C.

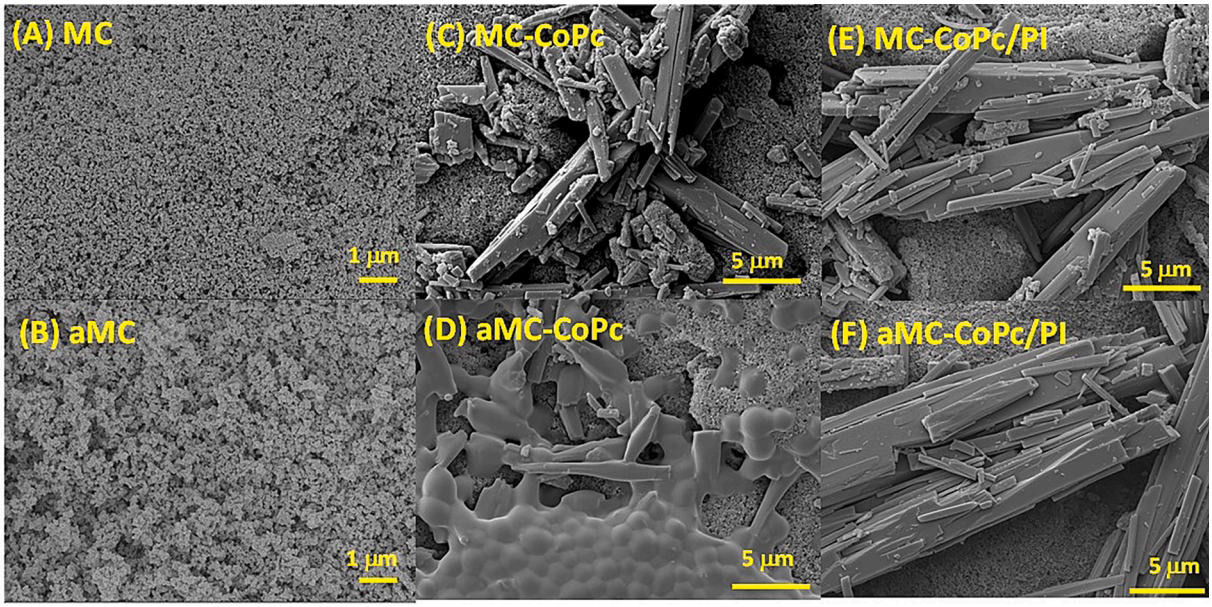

Fig. 2. SEM images of the MC (A), aMC (B), MC-CoPc (C), aMC-CoPc (D), MC-CoPc/PI (E) and aMC-CoPc/PI (F) at a magnification of 10,000 (A,B) and 5,000 (C-F).

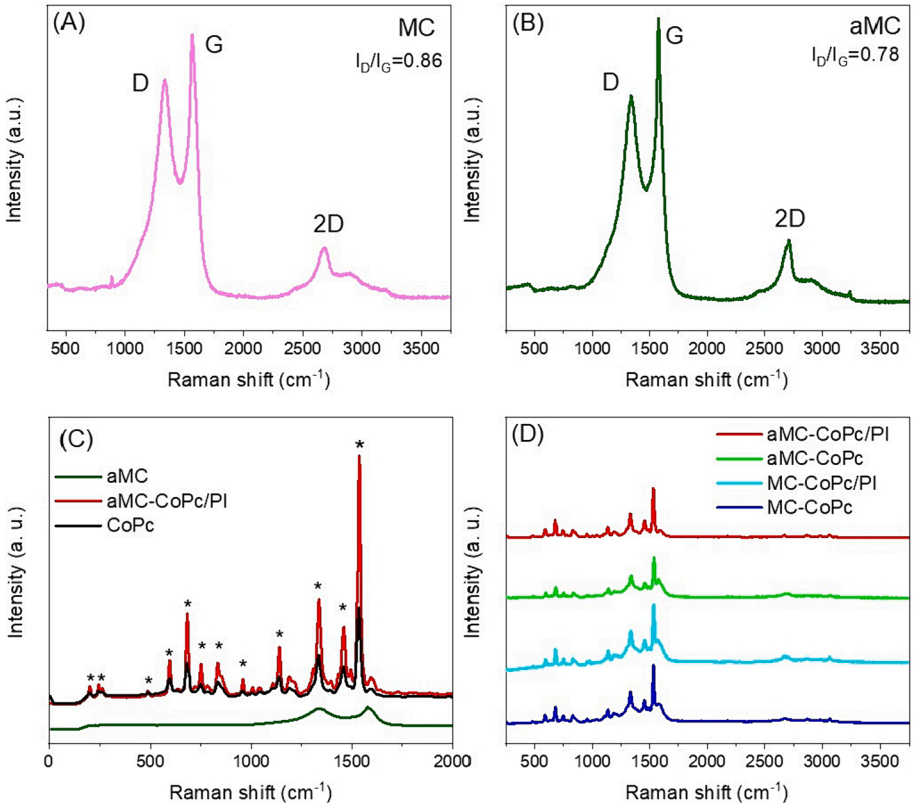

Fig. 3. Raman spectra of (A) MC, (B) aMC, (C) comparison between aMC, CoPc and aMC-CoPc/PI and (D) comparison between the different CoPc-modified electrodes.

The bands of CoPc appear at 200, 243, 485, 596, 683, 748, 833, 955, 1139, 1335, 1457 and 1533 cm^{-1}, as described in [50] (peaks marked with asterisks). There is an evident change in the Raman spectra of aMC before and after modification. aMC-CoPC/PI electrodes displayed a similar Raman spectrum to that of CoPc, which demonstrates the good deposition of CoPc on the mesoporous structure. A comparison between MC-CoPc, MC-CoPc/PI, aMC-CoPc and aMC-CoPc/PI electrodes is shown in Fig. 3D. The spectra demonstrate the presence of CoPc in all surfaces, with no significant differences. An overlapping in the bands of CoPc and graphite occurs, which makes the evaluation of the D and G bands of graphite difficult.

The electron transfer properties of the different electrodes (MC, aMC, MC-CoPc, MC-CoPc/PI, aMC-CoPc and aMC-CoPc/PI) were also studied by CV and EIS (Fig. 4). Voltammograms showed similar electrochemical response for MC and aMC (Fig. 4A), with peak potential difference (ΔE_p) 92.6 mV and $I_{pa}/I_{pc} = 1.25$, which indicates good electron transfer and relatively high quasi-reversibility of the system (Table S1). In the case of modified electrodes (Fig. 4D and G), better electrochemical results were obtained for MC-CoPc/PI and aMC-CoPc/PI with respect to their counterparts generated in the absence of PI (MC-CoPc and aMC-CoPc, respectively), which again demonstrates that deposition of CoPc by PI is certainly advantageous. Peaks were not well-defined for MC-CoPc, which indicates much poorer electron transfer associated to lower CoPc adsorption when compared to MC-CoPc/PI, aMC-CoPc and aMC-CoPc/PI. The ΔEp values were 260, 121, 172 and 99 mV for MC-CoPc, MC-CoPc/PI, aMC-CoPc and aMC-CoPc/PI, respectively (Table S1). The I_{pa}/I_{pc} ratio values were ~1.2 for all the electrodes, except for MC-CoPc.

Fig. 4B, E and H display the Nyquist plots of the impedance data for the different electrodes adjusted to the modified Randles equivalent circuit (see Table S2, which also includes the apparent electron transfer rate constants, k_{app}). A diagram of this circuit is shown in Fig. 4B, where R_u is the solution resistance, R_{ct} is the charge transfer resistance, Z_W is the Warburg impedance and CPE is the constant phase element. MC and aMC showed a behavior close to an ideal conductor (Fig. 4B). However, after activation, R_{ct} slightly increased, with values of 16 and 318 Ω for MC and aMC, respectively. Regarding the electrodes modified with CoPc, the Nyquist plots (Fig. 4E and H) showed higher R_{ct} values for the electrodes generated without PI (8523 and 3535 Ω for MC-CoPc and aMC-CoPc, respectively), which noticeably decreased for those electrodes generated with PI (442 and 133 Ω for MC-CoPc/PI and aMC-CoPc/PI, respectively). Therefore, PI is a procedure that leads to electrodes with improved electron transfer kinetics and ion permeability, in agreement with CV and EIS measurements (Fig. 4D, E, G and H). The lower R_{ct} values obtained in the electrodes modified by PI indicates high electron transfer kinetics, as could be also confirmed by the higher apparent electron transfer rate constants (k_{app}, Table S2). It also suggests a small electron-tunnelling distance between the modified film and the carbonaceous surface, which may indicate a flat orientation of CoPc on carbon electrodes [51]. The aMC-CoPc/PI electrode exhibited the lowest R_{ct} and the highest k_{app} with a behavior close to an ideal conductor. Values of CPE in the modified electrodes (Table S2) were in the same order of magnitude for all the modified electrodes, except for MC-CoPc, which had a lower value. This result is consistent with Fig. S3(A), which showed a lower double layer capacitance in the range of 0.2 and 0.5 V, compared to the other electrodes.

In addition, Bode plots for the electrodes under study have been included (Fig. 4C, F and I). MC showed a maximum phase angle of ~40° at low frequencies, which indicates a certain capacitive behavior of the electrode. The electrochemical activation resulted in a peak at higher frequencies with a lower phase angle, which could indicate a relaxation process of the interface with slower electronic transfer kinetics, which is consistent with the increase in R_{ct} and the decrease in k_{app} after the activation (Table S2).

The Bode plots of the CoPc-modified electrodes are displayed in Fig. 4F and I. In the case of MC-CoPc and aMC-CoPc, symmetrical peaks

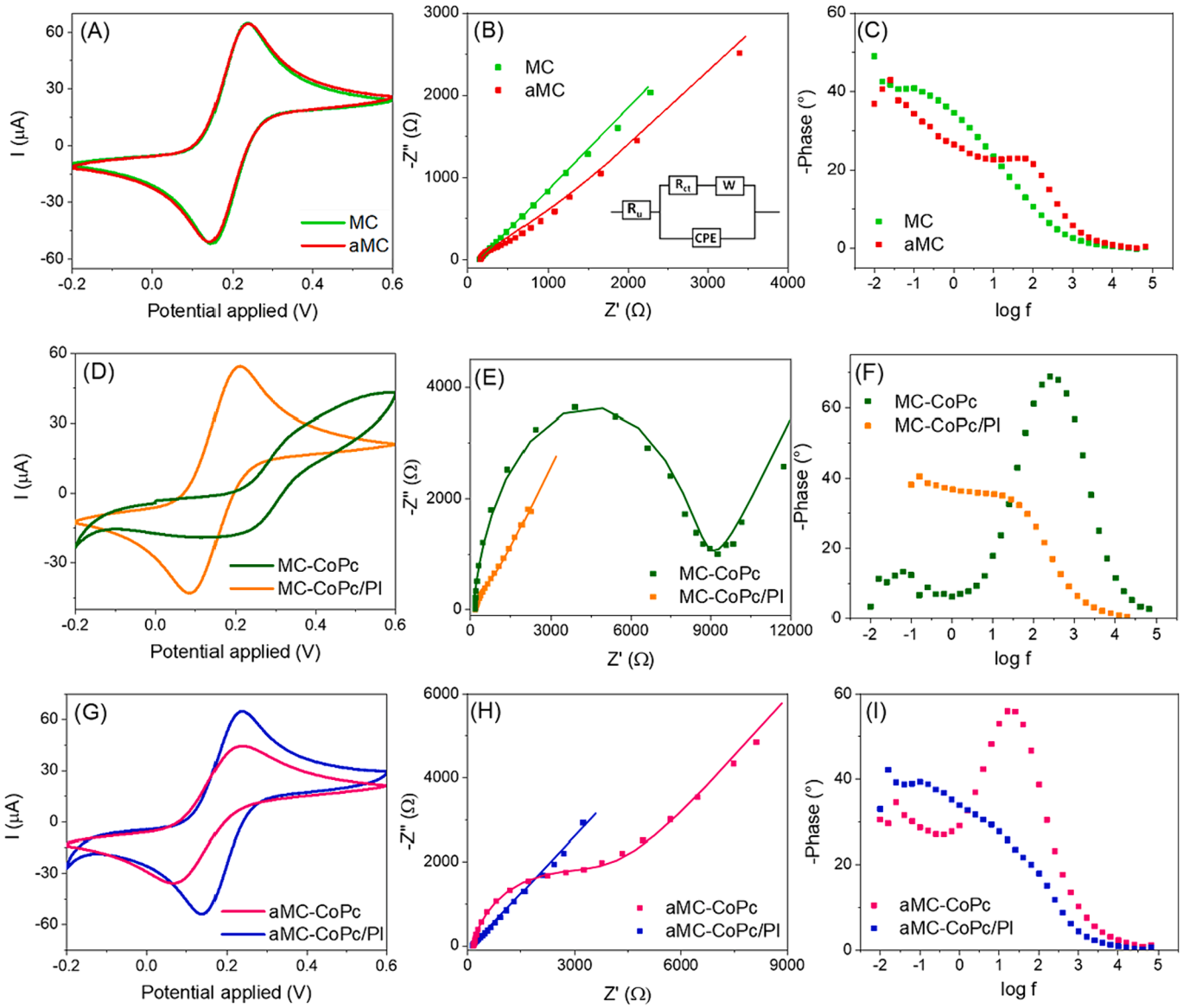

Fig. 4. CV response of 5.0 mM $K_4[Fe(CN)_6]$ in 0.1 M KCl at 50 mV·s^{-1} for the electrodes indicated on each panel (A, D, G). Nyquist plots (B, E, H). Bode plots (C, F, I).

were observed at high frequency with a maximum angle of 55-70°, corresponding to a relaxation process associated with interface phenomena. These results demonstrate poorer electron transfer and ion permeability of these electrodes, in agreement with the increase in R_{ct} (Table S2). Regarding the electrodes modified using PI, these symmetrical peaks disappeared, showing ill-defined peaks with lower phase angle shifted to lower frequencies. These results could indicate that the electronic transfer takes place on the CoPc film rather than on the aMC surface [51]. The higher coverage with CoPc revealed by SEM-EDX color mapping and the estimation of Γ in electrodes modified with PI could be consistent with all these claims (Figs. S2 and S3). In view of these results, the aMC-CoPc/PI electrode was considered to have the best electrochemical properties.

The double layer capacitance, which is related to the available surface area and porous characteristics of electrode materials [52] was studied for the electrodes bare SPCE (for comparative purposes), MC, aMC and aMC-CoPc/PI. The electrical double layer capacitance (Cdl) was calculated from the CVs recorded at different scan rates (Fig. S4). As expected, MCs showed higher Cdl than SPCEs (3.6 *vs.* 0.5 μF, respectively), due to the significant increase in porosity. Besides, activation with NaOH also led to an increase in Cdl (7.1 μF), in agreement with the increase in porosity observed by SEM (Fig. 2) and the presence of oxygen functional groups on the surface of the carbon-based active material [52] (Fig. 1). aMC-CoPc/PI showed an important increase in capacitance (51 μF), which could be due to the construction of a three-dimensional structure of CoPc able to store higher quantities of charge between layers [10]. The comparison of CVs displays how the capacitance increases with the successive treatments of MC (Fig. S4E). The results obtained can be related to an important increase in the electrochemical surface area (ECSA) of the electrodes.

Fig. S5 shows the change in cyclic voltammetry (0.1 M NaOH) before and after modification of the electrode (aMC-CoPc/PI). The response of the modified electrode revealed well-defined redox peaks potentials at –0.06 and 0.10 V (*vs.* Ag). These peaks correspond to the oxidation of $Co^{II}Pc$ to $Co^{II}(OH)_2Pc$ complex in the presence of OH^- from NaOH, and to the oxidation of $Co^{II}(OH)_2Pc$ to $Co^{III}(OOH)Pc$, respectively [33]. In addition, the peak potential at –0.2/–0.3 V corresponds to cobalt reduction [33] together with the electroreduction of O_2. Finally, an additional peak at approximately –0.5 V can be seen, which corresponds to the electroreduction of the porphyrin ring [33]. In addition, it can be appreciated that the reduction of O_2 (~–0.4 V at aMC) was shifted towards more positive potentials (–0.25 V at aMC-CoPc/PI). These results

agree with the fact that Co complexes, especially CoPc, are good electrocatalysts for the oxygen reduction reaction [53].

3.2. Electroanalytical figures of merit

The modified electrodes MC-CoPc, MC-CoPc/PI, aMC-CoPc and aMC-CoPc/PI were tested for the quantitative analysis of glucose by CV (Fig. 5). In all cases the electrochemical oxidation of glucose took place at potentials between 0.4 and 0.5 V. The mechanism involved consists of the oxidation of $Co^{II}Pc$ to $Co^{III}(OOH)Pc$, followed by glucose oxidation at the $Co^{III}(OOH)Pc$ active center of the electrode, as given by [33]:

$$Co^{III}(OOH)Pc + glucose \longrightarrow Co^{II}(OH)_2Pc + gluconolactone \quad (2)$$

The results obtained demonstrated that electrodes modified using PI exhibit higher peak intensities in the oxidation of glucose (Fig. 5B and D) compared to electrodes modified without PI (Fig. 5A and 5C). Furthermore, when MC-CoPc/PI and aMC-CoPc/PI are compared, better electroanalytical outcomes were achieved with the electrodes previously activated (Fig. 5D). These results could be related with an improved adsorption of CoPc in the presence of the salt, and they are in accordance with SEM, EDX, the estimation of electroactive CoPc concentration and the values of R_{ct} obtained by EIS (Figs. 2 and S2, calculation of Γ and Fig. 4).

In view of these results, the electrode aMC-CoPc/PI was chosen for analytical purposes. An optimization of the concentration of CoPc solution used for the carbonaceous modification can be seen in Fig. S6, with 2.5 mg/mL as the optimal concentration.

Fig. S7A shows the CVs of aMC-CoPc/PI in the presence of glucose at different scan rates. The peak current intensities at 0.1 V associated with cobalt oxidation were proportional to the scan rate (Fig. S7B), which indicates a surface reaction-controlled process (as also shown in Fig. S3). In contrast, the peaks associated with the oxidation of glucose (0.45 V) and reduction of cobalt (together with oxygen reduction) (–0.2 V) were proportional to the square root of scan rate, indicating diffusion-controlled processes (Figs. S7C and D).

The aMC-CoPc/PI electrode was successfully applied to glucose quantification by square wave voltammetry (SWV) (Fig. 6). SWV offers some advantages such as high sensitivity and selectivity and improved signal-to-noise ratio, making it easier to distinguish the signal from background noise. The corresponding voltammograms are shown in Fig. 6A, where a slight shift towards positive potentials was observed when glucose concentration was increased, probably due to the intermediate species coming from the oxidation of glucose which could partially be adsorbed on the surface of the electrode. The maximum current intensity for glucose oxidation was obtained at ~0.45 V (Fig. 6A) and a linear plot of the anodic peak current *vs* glucose concentration (Fig. 6B) was found. The sensitivity was 22.3 μA·mM^{-1}, the limit of detection (LoD) was 27.4 μM ($3\sigma/s$) and the limit of quantification 91.3 μM ($10\sigma/s$), being σ the standard deviation of the blank signal and *s* the sensitivity.

The repeatability of the proposed sensor was evaluated by performing five successive determinations with the same concentration of glucose (0.5 mM). The results showed a relative standard deviation (RSD) of 3.31 %. This value (<5%) indicates excellent repeatability and is similar to the values obtained with other non-enzymatic CoPc-based sensors [31–33]. Reproducibility of the electrode was also studied by

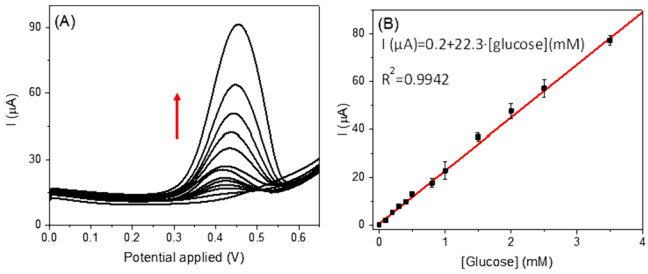

Fig. 6. (A) SWV responses of glucose standard solutions with increasing concentrations (0.1 to 3.5 mM) in 0.1 M NaOH using aMC-CoPc/PI. (B) Calibration plot recorded at the maximum peak current with glucose concentration; the error bars represent the standard deviation (n = 3).

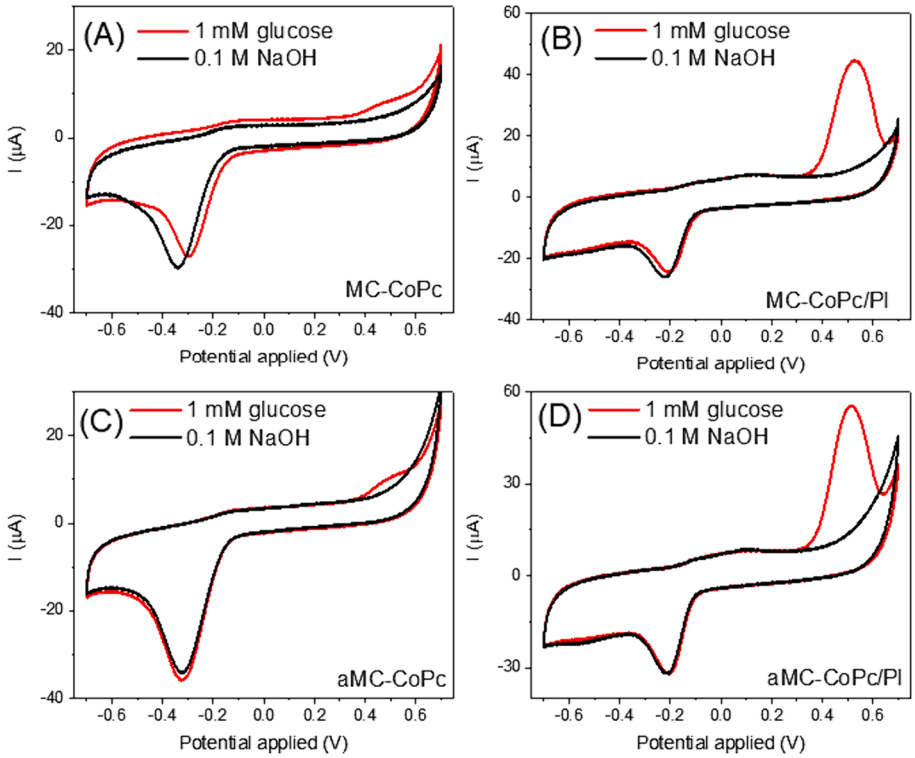

Fig. 5. CV response of MC-CoPc (A), MC-CoPc/PI (B), aMC-CoPc (C) and aMC-CoPc/PI (D) in the absence and presence of 1 mM glucose (50 mV·s^{-1}).

preparing five different electrodes and using them for the determination of 0.5 mM glucose, obtaining a RSD of 4.68 %. This value is in the same order of magnitude as the values reported for a glassy carbon electrode modified with multiwalled carbon nanotubes and cobalt tetrasulfonated phthalocyanine [31], and a pencil graphite electrode modified with overoxidized polypirrole nanofiber/cobalt phthalocyanine tetrasulfonate [54], and indicates a very good inter-electrode reproducibility of the modification herein proposed. To check stability, modified electrodes were stored at RT and the electrochemical response against 0.5 mM glucose was periodically recorded. The non-used electrodes retained 100 % of the signal after 2 months, which demonstrates outstanding stability and would allow the storage of these electrodes for long times at RT. In this sense, non-enzymatic sensors have a clear advantage over enzymatic biosensors, which, in addition to being more expensive, tend to be less stable and need to be stored under more specific conditions due to inactivation of enzymes [28].

The analytical parameters of the electrochemical sensor herein proposed were compared with other CoPc-based electrochemical glucose (bio)sensors found in bibliography (Table 1). The sensitivity of the aMC-CoPc/PI proposed in this work was better than most of the reported enzymatic and non-enzymatic (bio)sensors, except for reference [33], in which a glassy carbon electrode modified with a variety of sophisticated carbon nanomaterials (single-walled carbon nanotubes and reduced graphene oxide) was used. In terms of LoD, aMC-CoPc/PI exhibits a lower value than most enzymatic biosensors indicated in Table 1 [55,56], except for reference [57]. As regards non-enzymatic sensors, aMC-CoPc/PI achieved better LoD than the electrode made of pencil graphite and a conductive polymer [54], although electrodes including graphene showed lower LoD [32,33]. Regarding linear range, aMC-CoPc/PI electrode can quantify glucose from 0.1 to 3.5 mM, which is wider than most enzymatic biosensors indicated in Table 1. When compared with other non-enzymatic sensors, only the one that uses a CoPc derivative, namely CoPc tetrasulfonate (CoPcT), and DPV for the electrochemical measurements, presents a wider linear range [54]; it should also be noted that other non-enzymatic sensors showed two calibration ranges for glucose determination [32,33], which could potentially lead to inaccurate glucose measurements when falling in the middle of these two calibration ranges. To sum up, the electrode herein proposed, aMC-CoPc/PI, achieves good analytical performance at low potential (0.45 V) with no additional conductive material other than the MC screen-printed electrode and CoPc as electrocatalyst, making it a very simple electrode for mass production.

Selectivity of a sensor is essential for practical applications. For that reason, the electrochemical response of aMC-CoPc/PI to some electroactive species that can coexist with glucose in complex biological fluids and other real samples was recorded by SWV (Fig. S8). Among the compounds tested, ascorbate, dopamine and uric acid exhibited peaks at less positive potentials (0.02, 0.08 and 0.1 V, respectively), which means that they will not interfere with the quantification of glucose at 0.45 V. Particularly, the measurement of glucose in the presence of uric acid is possible because the oxidation potentials of both compounds are sufficiently separated (about 0.35 V, Fig. S8C). Additionally, autooxidation of ascorbate and dopamine in alkaline media is well-known [58,59], which makes these compounds non-interfering under these conditions. The compounds sucrose, urea, citrate, dehydroascorbate and NaCl did not show any oxidation peak at the studied potential window, which could be interesting for the measurement of glucose levels in different kinds of real samples. These results confirmed the excellent selectivity of aMC-CoPc/PI for glucose quantification. A scheme of the mechanism of glucose oxidation by the aMC-CoPc/PI is depicted in Fig. S8D.

The accurate measurement of glucose in real samples such as biological fluids and commercial preparations is of paramount importance in terms of health and quality control. The applicability of aMC-CoPc/PI was addressed by measuring glucose in samples of different nature, with different matrices, particularly horse serum, intravenous glucose saline solution and culture medium for sperm cells (Table 2). The measurement

Table 1
Comparison of the analytical performance of various CoPc-based electrodes for glucose determination.

Electrode	Electrochemical method	Sensitivity ($\mu A \cdot mM^{-1}$)	LOD (μM)	Linear range (mM)	Ref.
CoPc/GOD/SPCE (enzymatic GOx)	Amperometry (0.5 V *vs* Ag)	1.12	200	0.2–5.0	[55]
GO-CoPc paper-based electrode (enzymatic GOx)	Amperometry (0.4 V *vs* Ag)	2.2	63	0.1–1.0	[56]
CNF-CoPc paper-based electrode (enzymatic GOx)	Amperometry (0.4 V *vs* Ag)	2.6	68	0.1–1.0	[56]
MWCNT-CoPc paper-based electrode (enzymatic GOx)	Amperometry (0.4 V *vs* Ag)	1.3	91	0.3–1.0	[56]
Nafion/GOD/nanoCoPc-Gr/GCE (enzymatic GOx)	Amperometry (0.5 V *vs*. SCE)	11.4	14.6	0.02–1.6	[57]
PG/OPPyNF/CoPcT (non-enzymatic)	DPV (0.35 V *vs*. Ag/AgCl)	5.7	100	0.2–20.0	[54]
CoPc/G/IL/SPCE (non-enzymatic)	Amperometry (0.7 V and 0.8 V *vs* Ag)	15.9 9.8	0.67	0.01–1.3 1.3–5.0	[32]
SWCNT/rGO/CoPc/GCE (non-enzymatic)	Amperometry (0.55 V *vs* Ag/AgCl)	34.3 61.7	0.12	0.003–0.5 0.5–5.0	[33]
aMC-CoPc/PI (non-enzymatic)	SWV (0.45 V *vs* Ag)	22.3	27.4	0.1–3.5	This work

CoPc/GOD/SPCE: Cobalt phthalocyanine/glucose oxidase/screen-printed carbon electrode; **GO-CoPc:** Graphene oxide-cobalt phthalocyanine; **CNF-CoPc:** Carbon nanofibers-cobalt phthalocyanine; **MWCNT-CoPc:** Multiwalled carbon nanotubes-cobalt phthalocyanine; **Nafion/GOD/nanoCoPc-Gr/GCE:** Nafion/Glucose oxidase/cobalt phthalocyanine nanorod-graphene nanocomposite/glassy carbon electrode; **PG/OPPyNF/CoPcT:** Pencil graphite/overoxidized polypirrole nanofiber/cobalt(II) phthalocyanine tetrasulfonate; **CoPc/G/IL/SPCE:** Cobalt phthalocyanine/graphene composite/ionic liquid/screen printed electrode; **SWCNT/rGO/CoPc/GCE:** Single-walled carbon nanotube/reduced graphene oxide/cobalt phthalocyanine/glassy carbon electrode.

Table 2
Determination of glucose concentration in different real samples by using the electrode aMC-CoPc/PI. Data were compared by using a standard enzymatic spectrophotometric method.

Sample	[Glucose] (mM) aMC-CoPc/PI	[Glucose](mM) Spectrophotometric method	Recovery (%)
Horse serum	3.71 ± 0.06	3.61 ± 0.07	102.7
Intravenous glucose saline solution (diluted 1:100)	2.68 ± 0.04	2.55 ± 0.03	105.0
Culture medium for sperm cells (diluted 1:40)	1.45 ± 0.04	1.45 ± 0.01	100.0

The trueness of the method was calculated using recovery. This parameter was calculated as the ratio of glucose concentration found by aMC-CoPc/PI*100 and glucose concentration found by the reference method [61].

of glucose in this last case is key because this compound is an essential supplement for sperm conservation and motility [60]. The values obtained were compared to those obtained by a specific standard spectrophotometric method (enzymatic kit for glucose determination). The results showed excellent accuracy in the measurement of glucose with recoveries between 100 and 105 %. Therefore, the electrode aMC-CoPc/PI could be applied for the analysis of glucose in complex samples with high performance.

4. Conclusions

The preparation of a non-enzymatic glucose electrochemical sensor has been designed by following a simple and cost-effective method based on the combination of both electrochemical activation of MC substrate of screen-printed carbon platforms and the use of phase inversion (PI) to increase surface energy of the electrode for the effective deposition of CoPc. Physicochemical characterization of the electrodes has been addressed as a function of the electrochemical pretreatment of MC surface and the use of PI for the immobilization of CoPc. Findings showed that PI is a very effective tool for depositing higher amounts of CoPc on the MC surface, and that the electrochemical outcome of glucose oxidation improves with prior activation of the MC surface. Under those premises, the aMC-CoPc/PI electrode exhibited excellent catalytical properties for the oxidation of glucose, with high sensitivity and selectivity, as well exceptional stability after two months with electrocatalytic retention of 100 %. The aMC-CoPc/PI electrochemical sensor herein developed has been successfully applied to the measurement of glucose within some complex real samples, with recoveries between 100 and 105 % when compared to a standard enzymatic spectrophotometric method. The methodology herein proposed could represent a promising alternative for mass production of glucose electrochemical sensors based on metal phthalocyanines, as well as it could also be useful for the immobilization of other (bio)molecules or (bio) electrocatalysts on porous carbonaceous surfaces.

Funding

This work was partially supported by the research project TED2021-129921B-C21 funded by MCIN/AEI/https://doi.org/10.13039/501100011033 and by the European Union NextGeneration EU/PRTR, and grant No. 2022-GRIN-34199 funded by the own research plan of the UCLM for applied research projects, co-financed by the European Fund for Regional Development (FEDER). The authors also want to acknowledge Ministerio de Ciencia, Innovación y Universidades (Spain) for the support through ELECTROBIONET (RED2022-134120-T) from MCIN/AEI/https://doi.org/10.13039/501100011033. MIGS is a postdoctoral researcher of the own research plan of the UCLM funded from the EU through the European Social Fund Plus (ESF+) (Ref. PI001523). RJP is the beneficiary of a postdoctoral contract associated with the indicated project from the MCIN/AEI. HK received a grant from Laboratoire of Physics of Materials: structure and properties (LR01ES15), University of Carthage (Tunisia), to perform a scientific internship at the UCLM.

CRediT authorship contribution statement

María-Isabel González-Sánchez: Investigation, Methodology, Formal analysis, Data curation, Validation, Writing – original draft;, Writing – review & editing. **Hanen Khadhraoui:** Investigation, Methodology, Validation. **Rebeca Jiménez-Pérez:** Investigation, Methodology, Formal analysis, Data curation. **Jesús Iniesta:** Conceptualization, Supervision, Methodology, Writing – review & editing, Funding acquisition. **Edelmira Valero:** Conceptualization, Validation, Resources, Supervision, Funding acquisition, Project administration, Writing – original draft, Writing – review & editing.

Declaration of competing interest

The authors declare that they have no known competing financial interests or personal relationships that could have appeared to influence the work reported in this paper.

Data availability

No data was used for the research described in the article.

Appendix A. Supplementary data

Supplementary data to this article can be found online at https://doi.org/10.1016/j.microc.2024.110314.

References

[1] A.B. Sorokin, Phthalocyanine metal complexes in catalysis, Chem. Rev. 113 (2013) 8152–8191, https://doi.org/10.1021/CR4000072/ASSET/IMAGES/CR4000072.SOCIAL.JPEG_V03.
[2] N. Hernández-Ibáñez, I. Sanjuán, M.Á. Montiel, C.W. Foster, C.E. Banks, J. Iniesta, l-Cysteine determination in embryo cell culture media using Co (II)-phthalocyanine modified disposable screen-printed electrodes, J Electrochem Chem 780 (2016) 303–310, https://doi.org/10.1016/J.JELECHEM.2016.09.028.
[3] M. Wang, L. Zhu, S. Zhang, Y. Lou, S. Zhao, Q. Tan, L. He, M. Du, A copper(II) phthalocyanine-based metallo-covalent organic framework decorated with silver nanoparticle for sensitively detecting nitric oxide released from cancer cells, Sens Actuators B Chem 338 (2021) 129826, https://doi.org/10.1016/J.SNB.2021.129826.
[4] K. Kantize, I.N. Booysen, A. Mambanda, Electrochemical sensing of acetaminophen using nanocomposites comprised of cobalt phthalocyanines and multiwalled carbon nanotubes, J Electrochem Chem 850 (2019) 113391, https://doi.org/10.1016/J.JELECHEM.2019.113391.
[5] S. Nantaphol, W. Jesadabundit, O. Chailapakul, W. Siangproh, A new electrochemical paper platform for detection of 8-hydroxyquinoline in cosmetics using a cobalt phthalocyanine-modified screen-printed carbon electrode, J Electrochem Chem 832 (2019) 480–485, https://doi.org/10.1016/J.JELECHEM.2018.11.055.
[6] L. Cui, T. Pu, Y. Liu, X. He, Layer-by-layer construction of graphene/cobalt phthalocyanine composite film on activated GCE for application as a nitrite sensor, Electrochim. Acta 88 (2013) 559–564, https://doi.org/10.1016/J.ELECTACTA.2012.10.127.
[7] X.F. Zhang, X. Shao, π–π binding ability of different carbon nano-materials with aromatic phthalocyanine molecules: Comparison between graphene, graphene oxide and carbon nanotubes, J. Photochem. Photobiol. A Chem. 278 (2014) 69–74, https://doi.org/10.1016/J.JPHOTOCHEM.2014.01.001.
[8] C. Liang, Z. Li, S. Dai, Mesoporous Carbon Materials: Synthesis and Modification, Angew. Chem. Int. Ed. 47 (2008) 3696–3717, https://doi.org/10.1002/ANIE.200702046.
[9] A. Casanova, J. Iniesta, A. Gomis-Berenguer, Recent progress in the development of porous carbon-based electrodes for sensing applications, Analyst 147 (2022) 767–783, https://doi.org/10.1039/D1AN01978C.
[10] D. Martín-Yerga, E.C. Rama, A. Costa-García, Electrochemical Characterization of Ordered Mesoporous Carbon Screen-Printed Electrodes, J. Electrochem. Soc. 163 (2016) B176–B179, https://doi.org/10.1149/2.0871605JES/XML.
[11] W. Xin, Y. Song, Mesoporous carbons: recent advances in synthesis and typical applications, RSC Adv. 5 (2015) 83239–83285, https://doi.org/10.1039/C5RA16864C.
[12] S. Mehdipour-Ataei, E. Aram, Mesoporous Carbon-Based Materials: A Review of Synthesis, Modification, and Applications, Catalysts 13 (2022) 2, https://doi.org/10.3390/CATAL13010002.
[13] M. Zhou, L. Shang, B. Li, L. Huang, S. Dong, The characteristics of highly ordered mesoporous carbons as electrode material for electrochemical sensing as compared with carbon nanotubes, Electrochem. Commun. 10 (2008) 859–863, https://doi.org/10.1016/J.ELECOM.2008.03.008.
[14] N. Hernández-Ibáñez, V. Montiel, A. Gomis-Berenguer, C. Ania, J. Iniesta, Effect of confinement of horse heart cytochrome c and formate dehydrogenase from Candida boidinii on mesoporous carbons on their catalytic activity, Bioprocess Biosyst. Eng. 44 (2021) 1699–1710, https://doi.org/10.1007/S00449-021-02553-3.
[15] N. Hernández-Ibáñez, A. Gomis-Berenguer, V. Montiel, C.O. Ania, J. Iniesta, Fabrication of a biocathode for formic acid production upon the immobilization of formate dehydrogenase from Candida boidinii on a nanoporous carbon, Chemosphere 291 (2022) 133117, https://doi.org/10.1016/J.CHEMOSPHERE.2021.133117.
[16] H. Jia, N. Shang, Y. Feng, H. Ye, J. Zhao, H. Wang, C. Wang, Y. Zhang, Facile preparation of Ni nanoparticle embedded on mesoporous carbon nanorods for non-enzymatic glucose detection, J. Colloid Interface Sci. 583 (2021) 310–320, https://doi.org/10.1016/J.JCIS.2020.09.051.
[17] M.A. Wahab, S.M.A. Hossain, M.K. Masud, H. Park, A. Ashok, M. Mustapić, M. Kim, D. Patel, M. Shahbazi, M.S.A. Hossain, Y. Yamauchi, Y.V. Kaneti,

Nanoarchitectured superparamagnetic iron oxide-doped mesoporous carbon nanozymes for glucose sensing, Sens Actuators B Chem 366 (2022) 131980, https://doi.org/10.1016/J.SNB.2022.131980.
[18] Z. Bilici, Y. Ozay, A. Yuzer, M. Ince, K. Ocakoglu, N. Dizge, Fabrication and characterization of polyethersulfone membranes functionalized with zinc phthalocyanines embedding different substitute groups, Colloids Surf A Physicochem Eng Asp 617 (2021) 126288, https://doi.org/10.1016/J.COLSURFA.2021.126288.
[19] S. Pérez, E. Fàbregas, Amperometric bienzymatic biosensor for L-lactate analysis in wine and beer samples, Analyst 137 (2012) 3854–3861, https://doi.org/10.1039/C2AN35227C.
[20] S. Sánchez, E. Fà, H. Iwai, M. Pumera, M. Pumera, S. Sánchez, E. Fà, H. Iwai, Phase-Inversion Method for Incorporation of Metal Nanoparticles into Carbon-Nanotube/Polymer Composites, Small 5 (2009) 795–799, https://doi.org/10.1002/SMLL.200801482.
[21] S. Sánchez, M. Pumera, E. Fàbregas, Carbon nanotube/polysulfone screen-printed electrochemical immunosensor, Biosens. Bioelectron. 23 (2007) 332–340, https://doi.org/10.1016/J.BIOS.2007.04.021.
[22] L. Kong, Q. Ma, Z. Xu, X. Shen, J. Wang, J. Zhu, Three-dimensional graphene network deposited with mesoporous nitrogen-doped carbon from non-solvent induced phase inversion for high-performance supercapacitors, J. Colloid Interface Sci. 558 (2020) 21–31, https://doi.org/10.1016/J.JCIS.2019.09.095.
[23] S. Choudhury, D. Fischer, P. Formanek, F. Simon, M. Stamm, L. Ionov, Porous carbon prepared from polyacrylonitrile for lithium-sulfur battery cathodes using phase inversion technique, Polymer (guildf) 151 (2018) 171–178, https://doi.org/10.1016/J.POLYMER.2018.07.026.
[24] S. Pérez, J. Bartrolí, E. Fàbregas, Amperometric biosensor for the determination of histamine in fish samples, Food Chem. 141 (2013) 4066–4072, https://doi.org/10.1016/J.FOODCHEM.2013.06.125.
[25] S. Sánchez, M. Roldán, S. Pérez, E. Fàbregas, Toward a fast, easy, and versatile immobilization of biomolecules into carbon nanotube/polysulfone-based biosensors for the detection of hCG hormone, Anal. Chem. 80 (2008) 6508–6514, https://doi.org/10.1021/AC7025282/SUPPL_FILE/AC7025282-FILE002.PDF.
[26] S. Sánchez, E. Fàbregas, M. Pumera, Detection of biomarkers with carbon nanotube-based immunosensors, Methods Mol. Biol. 625 (2010) 227–237, https://doi.org/10.1007/978-1-60761-579-8_19/COVER.
[27] S. Park, H. Boo, T.D. Chung, Electrochemical non-enzymatic glucose sensors, Anal. Chim. Acta 556 (2006) 46–57, https://doi.org/10.1016/J.ACA.2005.05.080.
[28] D.W. Hwang, S. Lee, M. Seo, T.D. Chung, Recent advances in electrochemical non-enzymatic glucose sensors – A review, Anal. Chim. Acta 1033 (2018) 1–34, https://doi.org/10.1016/J.ACA.2018.05.051.
[29] F. Jiménez-Fiérrez, M.I. González-Sánchez, R. Jiménez-Pérez, J. Iniesta, E. Valero, Glucose Biosensor Based on Disposable Activated Carbon Electrodes Modified with Platinum Nanoparticles Electrodeposited on Poly(Azure A), Sensors (basel) 20 (2020) 1–15, https://doi.org/10.3390/S20164489.
[30] R. Wang, X. Liu, Y. Zhao, J. Qin, H. Xu, L. Dong, S. Gao, L. Zhong, Novel electrochemical non-enzymatic glucose sensor based on 3D Au@Pt core–shell nanoparticles decorated graphene oxide/multi-walled carbon nanotubes composite, Microchem. J. 174 (2022) 107061, https://doi.org/10.1016/J.MICROC.2021.107061.
[31] R. Devasenathipathy, C. Karuppiah, S.M. Chen, S. Palanisamy, B.S. Lou, M.A. Ali, F. M.A. Al-Hemaid, A sensitive and selective enzyme-free amperometric glucose biosensor using a composite from multi-walled carbon nanotubes and cobalt phthalocyanine, RSC Adv. 5 (2015) 26762–26768, https://doi.org/10.1039/C4RA17161F.
[32] S. Chaiyo, E. Mehmeti, W. Siangproh, T.L. Hoang, H.P. Nguyen, O. Chailapakul, K. Kalcher, Non-enzymatic electrochemical detection of glucose with a disposable paper-based sensor using a cobalt phthalocyanine–ionic liquid–graphene composite, Biosens. Bioelectron. 102 (2018) 113–120, https://doi.org/10.1016/J.BIOS.2017.11.015.
[33] O. Adeniyi, N. Nwahara, D. Mwanza, T. Nyokong, P. Mashazi, Nanohybrid electrocatalyst based on cobalt phthalocyanine-carbon nanotube-reduced graphene oxide for ultrasensitive detection of glucose in human saliva, Sens Actuators B Chem 348 (2021) 130723, https://doi.org/10.1016/J.SNB.2021.130723.
[34] M.R. Fernández-Santos, F. Martínez-Pastor, V. García-Macías, M.C. Esteso, A. J. Soler, P. Paz, L. Anel, J.J. Garde, Sperm Characteristics and DNA Integrity of Iberian Red Deer (Cervus elaphus hispanicus) Epididymal Spermatozoa Frozen in the Presence of Enzymatic and Nonenzymatic Antioxidants, J. Androl. 28 (2007) 294–305, https://doi.org/10.2164/JANDROL.106.000935.
[35] M.I. González-Sánchez, B. Gómez-Monedero, J. Agrisuelas, J. Iniesta, E. Valero, Highly activated screen-printed carbon electrodes by electrochemical treatment with hydrogen peroxide, Electrochem. Commun. 91 (2018) 36–40, https://doi.org/10.1016/J.ELECOM.2018.05.002.
[36] M.I. González-Sánchez, B. Gómez-Monedero, J. Agrisuelas, J. Iniesta, E. Valero, Electrochemical performance of activated screen printed carbon electrodes for hydrogen peroxide and phenol derivatives sensing, J Electrochem Chem 839 (2019) 75–82, https://doi.org/10.1016/J.JELECHEM.2019.03.026.
[37] W.Y. Su, S.M. Wang, S.H. Cheng, Electrochemically pretreated screen-printed carbon electrodes for the simultaneous determination of aminophenol isomers, J Electrochem Chem 651 (2011) 166–172, https://doi.org/10.1016/J.JELECHEM.2010.11.028.
[38] M.I. González-Sánchez, M.I. Romero-Llapa, B. Gómez-Monedero, R. Jiménez-Pérez, J. Iniesta, E. Valero, A Fast and Simple Ozone-mediated Method towards Highly Activated Screen Printed Carbon Electrodes as Versatile Electroanalytical Tools, Electroanalysis 31 (2019) 2299–25545, https://doi.org/10.1002/elan.201900335.
[39] E. Mazzotta, S. Rella, A. Turco, C. Malitesta, XPS in development of chemical sensors, RSC Adv. 5 (2015) 83164–83186, https://doi.org/10.1039/C5RA14139G.
[40] L. Zhao, Y. Li, M. Yu, Y. Peng, F. Ran, Electrolyte-Wettability Issues and Challenges of Electrode Materials in Electrochemical Energy Storage, Energy Conversion, and beyond, Adv Sci 10 (2023) 2300283, https://doi.org/10.1002/ADVS.202300283.
[41] T. Schmitt, P. Ferstl, L. Hammer, M.A. Schneider, J. Redinger, Adsorption and Intermolecular Interaction of Cobalt Phthalocyanine on CoO(111) Ultrathin Films: An STM and DFT Study, J. Phys. Chem. C 121 (2017) 2889–2895, https://doi.org/10.1021/ACS.JPCC.6B12337.
[42] A. Vinu, P. Srinivasu, M. Takahashi, T. Mori, V.V. Balasubramanian, K. Ariga, Controlling the textural parameters of mesoporous carbon materials, Microporous and Mesoporous Mat 100 (2007) 20–26, https://doi.org/10.1016/J.MICROMESO.2006.10.008.
[43] N.M.S. Hidayah, W.-W. Liu, C.-W. Lai, N.Z. Noriman, C.-S. Khe, U. Hashim, H. C. Lee, Comparison on graphite, graphene oxide and reduced graphene oxide: Synthesis and characterization, AIPC 1892 (2017) 150002, https://doi.org/10.1063/1.5005764.
[44] A.K. Singh, N. Yasri, K. Karan, E.P.L. Roberts, Electrocatalytic Activity of Functionalized Carbon Paper Electrodes and Their Correlation to the Fermi Level Derived from Raman Spectra, ACS Appl Energy Mater 2 (2019) 2324–2336, https://doi.org/10.1021/ACSAEM.9B00180/ASSET/IMAGES/LARGE/AE-2019-00180F_0006.JPEG.
[45] A.K. Sundramoorthy, S. Gunasekaran, Partially Oxidized Graphene/Metallic Single-Walled Carbon Nanotubes Film-Coated Electrode for Nanomolar Detection of Dopamine, Electroanalysis 27 (2015) 1811–1816, https://doi.org/10.1002/ELAN.201500047.
[46] C. Casiraghi, S. Pisana, K.S. Novoselov, A.K. Geim, A.C. Ferrari, Raman fingerprint of charged impurities in graphene, Appl. Phys. Lett. 91 (2007) 233108, https://doi.org/10.1063/1.2818692/334257.
[47] A. Das, S. Pisana, B. Chakraborty, S. Piscanec, S.K. Saha, U.V. Waghmare, K. S. Novoselov, H.R. Krishnamurthy, A.K. Geim, A.C. Ferrari, A.K. Sood, Monitoring dopants by Raman scattering in an electrochemically top-gated graphene transistor, Nat. Nanotechnol. 3 (2008) 210–215, https://doi.org/10.1038/nnano.2008.67.
[48] A. Mishra, Z. Ahmad, I. Zimmermann, D. Martineau, R.A. Shakoor, F. Touati, K. Riaz, S.A. Al-Muhtaseb, M.K. Nazeeruddin, Effect of annealing temperature on the performance of printable carbon electrodes for perovskite solar cells, Org. Electron. 65 (2019) 375–380, https://doi.org/10.1016/J.ORGEL.2018.11.046.
[49] H. Cao, X. Peng, M. Zhao, P. Liu, B. Xu, J. Guo, Oxygen functional groups improve the energy storage performances of graphene electrochemical supercapacitors, RSC Adv. 8 (2018) 2858–2865, https://doi.org/10.1039/C7RA12425B.
[50] J. Jia, X. Zhao, W. Hu, Y. Wang, J. Huang, J. Huang, H. Li, Y. Peng, H. Ma, C. Xu, Role of cobalt phthalocyanine on the formation of high-valent cobalt species revealed by in situ Raman spectroscopy, J Mater Chem A Mater 11 (2023) 8141–8149, https://doi.org/10.1039/D2TA10063K.
[51] K.I. Ozoemena, Anodic oxidation and amperometric sensing of hydrazine at a glassy carbon electrode modified with cobalt (II) phthalocyanine–cobalt (II) tetraphenylporphyrin (CoPc- (CoTPP)4) supramolecular complex, Sensors 6 (2006) 874–891, https://doi.org/10.3390/S6080874.
[52] A.G. Olabi, Q. Abbas, M.A. Abdelkareem, A.H. Alami, M. Mirzaeian, E.T. Sayed, Carbon-based materials for supercapacitors: recent progress, Challenges and Barriers, Batteries 9 (2023) 19, https://doi.org/10.3390/BATTERIES9010019.
[53] W. Zhou, H. Yadegari, E.A. Ticianelli, F. Tasca, M. Viera, J. Riquelme, C. Aliaga, J. F. Marco, W. Orellana, J.H. Zagal, Oxygen reduction reaction at penta-coordinated Co phthalocyanines, Front. Chem. 1 (2020) 22, https://doi.org/10.3389/fchem.2020.00022.
[54] L. Özcan, Y. Şahin, H. Türk, Non-enzymatic glucose biosensor based on overoxidized polypyrrole nanofiber electrode modified with cobalt(II) phthalocyanine tetrasulfonate, Biosens. Bioelectron. 24 (2008) 512–517, https://doi.org/10.1016/J.BIOS.2008.05.004.
[55] E. Crouch, D.C. Cowell, S. Hoskins, R.W. Pittson, J.P. Hart, Amperometric, screen-printed, glucose biosensor for analysis of human plasma samples using a biocomposite water-based carbon ink incorporating glucose oxidase, Anal. Biochem. 347 (2005) 17–23, https://doi.org/10.1016/J.AB.2005.08.011.
[56] A. Sánchez-Calvo, A. Costa-García, M.C. Blanco-López, Paper-based electrodes modified with cobalt phthalocyanine colloid for the determination of hydrogen peroxide and glucose, Analyst 145 (2020) 2716, https://doi.org/10.1039/c9an02413a.
[57] H. Wang, Y. Bu, W. Dai, K. Li, H. Wang, X. Zuo, Well-dispersed cobalt phthalocyanine nanorods on graphene for the electrochemical detection of hydrogen peroxide and glucose sensing, Sens Actuators B Chem 216 (2015) 298–306, https://doi.org/10.1016/J.SNB.2015.04.044.
[58] S. Schindler, T. Bechtold, Mechanistic insights into the electrochemical oxidation of dopamine by cyclic voltammetry, J Electrochem Chem 836 (2019) 94–101, https://doi.org/10.1016/j.jelechem.2019.01.069.
[59] X. Yin, K. Chen, H. Cheng, X. Chen, S. Feng, Y. Song, L. Liang, Chemical stability of ascorbic acid integrated into commercial products: a review on bioactivity and delivery chemical stability of ascorbic acid integrated into commercial products: a

review on bioactivity and delivery technology, Antioxidants 11 (2022) 153, https://doi.org/10.3390/antiox11010153.
[60] A. Amaral, C. Paiva, M. Baptista, A.P. Sousa, J. Ramalho-Santos, Exogenous glucose improves long-standing human sperm motility, viability, and mitochondrial function, Fertil. Steril. 96 (2011) 848–850, https://doi.org/10.1016/J.FERTNSTERT.2011.07.1091.
[61] F. Raposo, C. Ibelli-Bianco, Performance parameters for analytical method validation: Controversies and discrepancies among numerous guidelines, Trends Anal. Chem. 129 (2020) 115913, https://doi.org/10.1016/j.trac.2020.115913.